Supporting Information

Electrostatic and Charge-Induced Methane Activation by a Concerted Double C–H Bond Insertion

Caiyun Geng,[1] Jilai Li,[1,2,*] Thomas Weiske,[1] Maria Schlangen,[1] Sason Shaik,[3,*] Helmut Schwarz,[1,*]

[1]Institut für Chemie, Technische Universität Berlin, Straße des 17. Juni 135, 10623 Berlin, Germany

[2]Institute of Theoretical Chemistry, Jilin University, Changchun 130023, People's Republic of China

[3]Institute of Chemistry and the Lise-Meitner-Minerva Center for Computational Quantum Chemistry, The Hebrew University of Jerusalem, 91904 Jerusalem, Israel

*Correspondence and requests for further materials should be addressed to H.S. (Helmut.Schwarz@tu-berlin.de), to S.S. (Sason@yfaat.ch.huji.ac.il), or to J.L. (Jilai@jlu.edu.cn)

Table of Content

1. Experimental details

The ion/molecule reactions were performed with a Spectrospin CMS 47X Fourier transform ion cyclotron resonance (FT-ICR) mass spectrometer equipped with an external ion source as described elsewhere.[1-3] In brief, $[Cu–C]^+$ was generated by laser ablation of a Cu/graphite disk using a Nd:YAG laser operating at 1064 nm seeded in helium; the latter serves as carrier gas. Using a series of potentials and ion lenses, the ions were transferred into the ICR cell, which is positioned in the bore of a 7.05 T superconducting magnet. After proper thermalization by pulses of argon (ca. 2×10^{-6} mbar), the reactions of mass-selected $[Cu–C]^+$, m/z = 75, were studied by introducing isotopologues of methane, i.e. CH_4, CD_4, and CH_2D_2, via a leak valve at stationary pressures. A temperature of 298 K for the thermalized species was assumed.[1-3]

2. Computational details

All electronic structure calculations were performed with the Gaussian 09 package.[4] Unless stated otherwise, we used the B2PLYP[5] double hybrid density functional. For geometry optimization we used the augmented correlation-consistent polarized triple zeta (Aug-cc-pVTZ) basis set with implicit treatment of scalar-relativistic effects by using the effective core potential (ECP) pseudopotential for the metal atoms,[6] and the cc-pVTZ all-electron basis set for all other atoms[7] (BSI). Harmonic vibrational frequencies were computed to verify the nature of the stationary points. The minimum structures reported in this publication show only positive eigenvalues of the Hessian matrix, whereas the transition states have one negative eigenvalue. Intrinsic reaction coordinate[8-11] calculations were also performed to confirm that the transition states correlate with the designated intermediates.

The zero-point vibrational energy (ZPVE) and thermal corrections to the enthalpy were calculated for structures optimized at the B2PLYP/BSI level. The thermodynamic functions (ΔH) were estimated within the ideal gas, rigid-rotor, and harmonic oscillator approximations at 298K and 1 atm.

To refine the energies, single point energy (SPE) calculations at the CCSD(T)/BSII//B2PLYP/BSI level were carried out, where BSII involves an aug-cc-pVQZ all-electron basis set for the carbon, and hydrogen atoms,[7] and the aug-cc-pVQZ-ECP for the metal atoms.[6] Douglas-Kroll-Hess 2nd order scalar relativistic effects were considered in these calculations.[12] This level of theory has been shown earlier to provide chemical accuracy in the calculations of reaction energies, barriers and weak interactions.[13-16]

For the $[Cu–C]^+/CH_4$ system, we note that the PBE1PBE,[17] M06,[18] M11,[19] M11L,[20] BHandHLYP,[21] B2GP-PLYP[22] and MP2[23] methods in conjunction with BSI were also used to re-optimize most of the structures, especially the transition structure **^{1}TS-diH**, to ensure the quality of the results given by single DFT method.

A comparison between the DFT methods B2PLYP, B2GP-PLYP and CCSD(T) is given in Table S1. It can be seen that the results obtained by the B2PLYP method are reliable.

Since the synchronous insertion of a carbon atom into two C–H bonds of methane for $[Au–C]^+$ was not considered in our previous study,[24] we re-examined the $[Au–C]^+/CH_4$ system with respect to this mechanism. However, the traditional strategy for locating this transition state turned out to be rather difficult. Therefore, we performed a series of 3-dimensional (3D) scans by fixing the distances of the C–C_{met} and two C–H_t bonds. Here C refers to the carbon atom of $[Au–C]^+$, C_{met} is the carbon atom of methane, and H_t is the hydrogen atom in transit. The two C–H bonds were fixed at the same value, and the structures confined to C_s symmetry. We also carried out a series of 3D scans with relaxed C–H bonds with two angles of C_{met}–C–H_t remained fixed. In these scans, the step size for the C–C bond is set to 0.02 Å in the range of 2.0 Å to 1.4 Å, for the C–H bonds to 0.01 Å from 1.6 Å to 1.1 Å, and for the angles of C_{met}–C–H_t to 1° in the range of 50° to 70. Near the "saddle point", the energetic difference between two adjacent grids amounts to less than 1.0 kJ/mol. The same structure for the saddle point was obtained by these two scan set-ups. These scans were performed at the B2PLYP/BSI level of theory.

Balucani and coworkers calculated the potential energy surfaces of the $C(^1D)/CH_4$ system at the CCSD(T)/Aug-cc-pVTZ//B3LYP/Aug-cc-pVTZ level of theory.[25] These authors stated that singlet $C(^1D)$ reacts with methane via a direct insertion of the carbon atom into one of the C–H bonds resulting in the barrier free formation of the intermediate $HCCH_3$. Whereas a relaxed scan on making the C–C bond at the B3LYP/Aug-cc-pVTZ level of theory shows a downhill surface, energy refinement on these B3LYP-derived structures along the scan at the CCSD(T)/Aug-cc-pVTZ level provides, however, a rather different picture: there exists a "hill" during the insertion process indicating that there might exist a transition state (TS).

To locate this TS for $C(^1D)/CH_4$, we re-scanned the insertion process at the QCISD/cc-pVTZ level of theory, and then subjected the top point to a transition state locating procedure. Finally, a true transition state was successfully identified. In addition, this transition state can also be located at the QCISD/Aug-cc-pVTZ, CCSD/cc-pVTZ, B2PLYP/cc-pVTZ levels of theory. Thus, the insertion of a carbon atom into the C–H bond of methane corresponds, actually, to a stepwise instead of a direct process as proposed earlier.[25] The corresponding potential energy surface and the structures involved in this mechanistic scenario of the $C(^1D)/CH_4$ reaction are provided in Figure S4.

The synchronous insertion of $C(^1D)$ into two C–H bonds of methane has not been considered previously. Therefore, we employed the same strategy, mentioned above for the $[Au–C]^+/CH_4$ couple to locate the saddle point; the result is shown in Figure S9.

Deformation energies (ΔE_{def}) were calculated at the B2PLYP/BSI level for the respective transition states and were plotted against the respective barriers ($\Delta E^{\neq}$) as a diagnostic tool.[26] ΔE_{def} refers to the energy spent by the reactants to reach the structure adopted in the transition state, respectively, namely $\Delta E_{def} = E(CH_4 + [Cu–C]^{\bullet+}$ at TS geometry) – E(EC); the respective barriers are the electronic barrier without corrections for zero-point vibrational energy or any thermal contributions. To avoid negative barriers, the energy of the encounter complex was used as a reference state.

The barrier is related to the deformation energy as follows:[13,26-38]

$$\Delta E^{\neq} = \Delta E_{def} + \Delta E_{int}$$

ΔE_{int} corresponds the total interaction energy, contributed by repulsive interactions (e.g., Pauli repulsion) and stabilizing interactions (electrostatic, polarization, and bonding). The line in the Figure S8 has a slope of unity with $\Delta E^{\neq} = \Delta E_{def}$.

Natural bond orbital[39-44] calculations were performed to obtain further information of selected stationary points along reaction coordinates by using NBO 6.[45] Quasi-restricted orbitals analysis[46,47] were carried out by using ORCA.[48]

3. The C(^{1}D)/CH_4 reaction

The QCISD and CCSD optimized potential energy surfaces for the insertion of C(^{1}D) in one C-H bond is shown in Figure S4. It can be seen that a loosely bound encounter complex, **^{1}EC**, is formed in the association step. Subsequently, the carbon atom abstracts one of the hydrogen from methane via surmounting transition state **^{1}TS-HT** (9 kJ mol^{-1}), giving rise to the $HCCH_3$ intermediate. Note that this transition state can also be located at the B2PLYP/BSI level of theory. For the sake of consistency, we use the B2PLYP-optimized structures for our discussion in the main text.

4. FIGURE

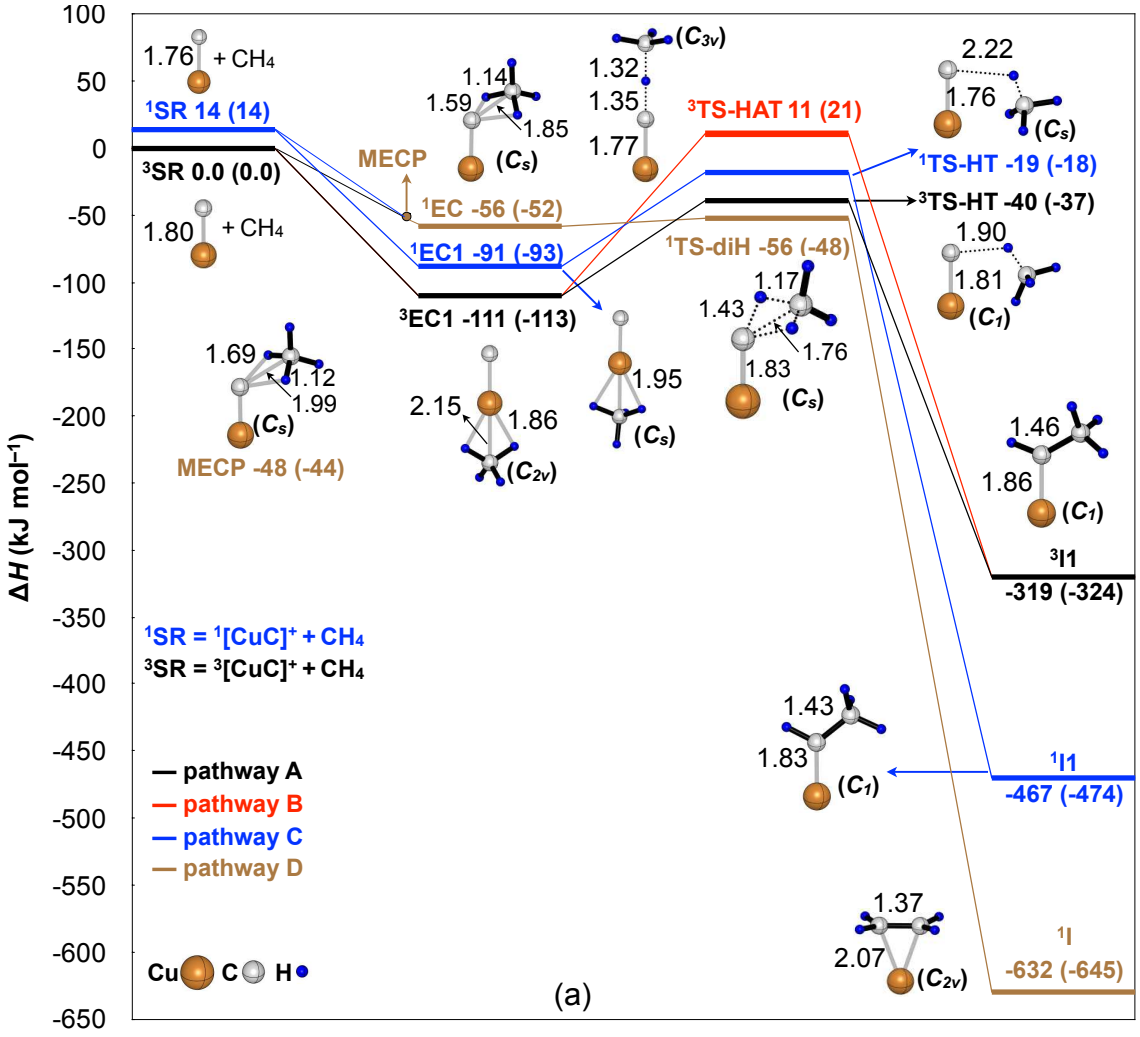
ΔH (kJ mol⁻¹)
100
50
0
-50
-100
-150
-200
-250
-300
-350
-400
-450
-500
-550
-600
-650
1.76 + CH4
1SR 14 (14)
3SR 0.0 (0.0)
1.80 + CH4
1.69
1.12
1.99
(Cs)
MECP -48 (-44)
MECP
1.14
1.59
1.85
(Cs)
1EC -56 (-52)
1EC1 -91 (-93)
3EC1 -111 (-113)
2.15
1.86
(C2v)
1.95
(Cs)
(C3v)
1.32
1.35
1.77
3TS-HAT 11 (21)
1TS-diH -56 (-48)
1.17
1.43
1.76
1.83
(Cs)
2.22
1.76
(Cs)
1TS-HT -19 (-18)
3TS-HT -40 (-37)
1.90
1.81
(C1)
1.46
1.86
(C1)
3I1
-319 (-324)
1SR = 1[CuC]+ + CH4
3SR = 3[CuC]+ + CH4
pathway A
pathway B
pathway C
pathway D
Cu C H
1.43
1.83
(C1)
1I1
-467 (-474)
1.37
2.07
(C2v)
1I
-632 (-645)
(a)

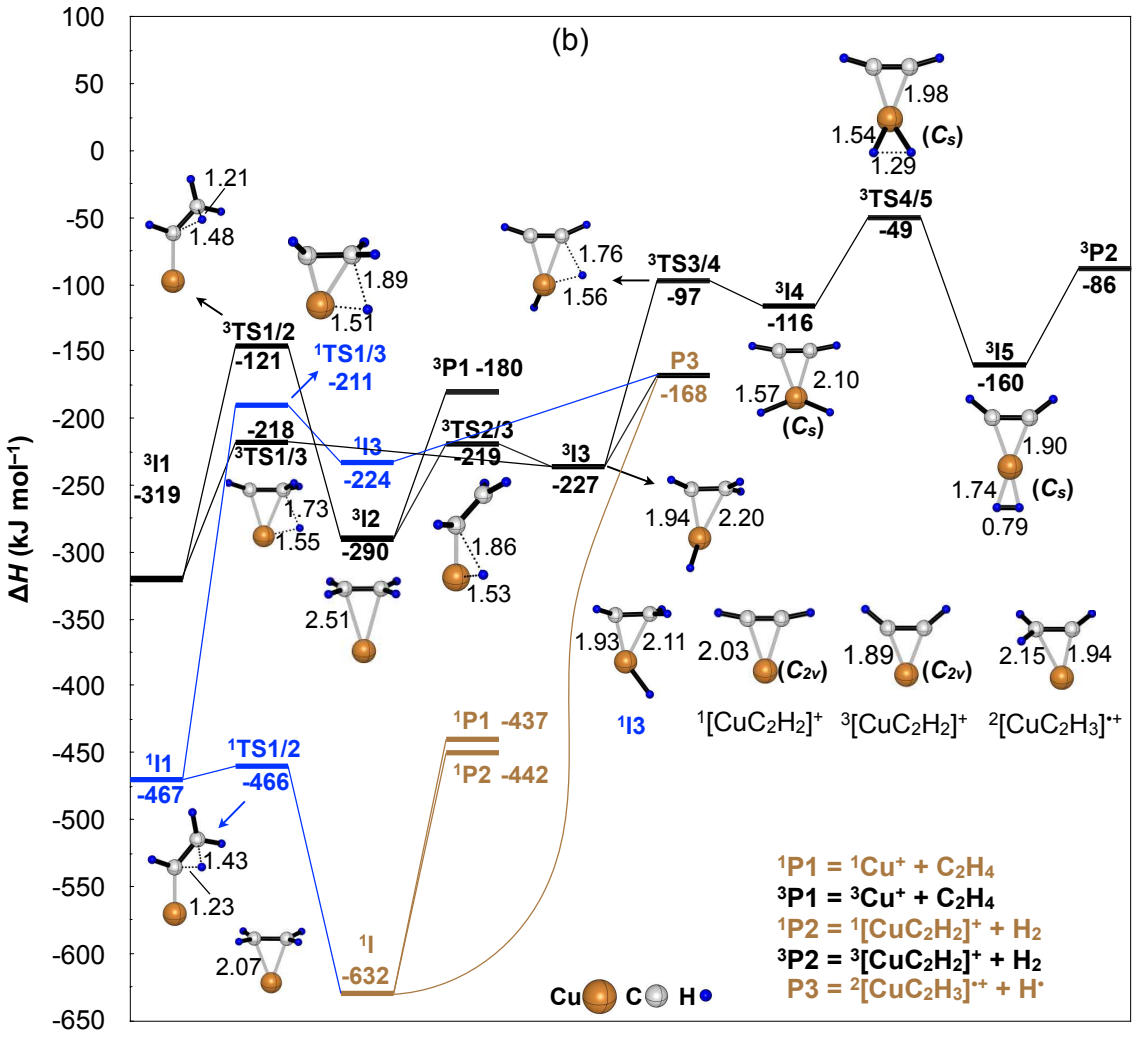

Figure S1. CCSD(T)//B2PLYP-calculated potential energy profiles for the C–H bond insertions (a) and the dissociation processes (b) in the reaction of $[Cu–C]^+$ with CH_4. Key ground-state structures with selected geometric parameters are also provided. The relative enthalpies (ΔH_{298K} in kJ mol^{-1}), corrected for contributions of zero-point vibrational energy and thermal corrections, of the reaction intermediates and transition states are given relative to the separated reactants $[Cu–C]^+$ and CH_4. Charges are omitted for the sake of clarity.

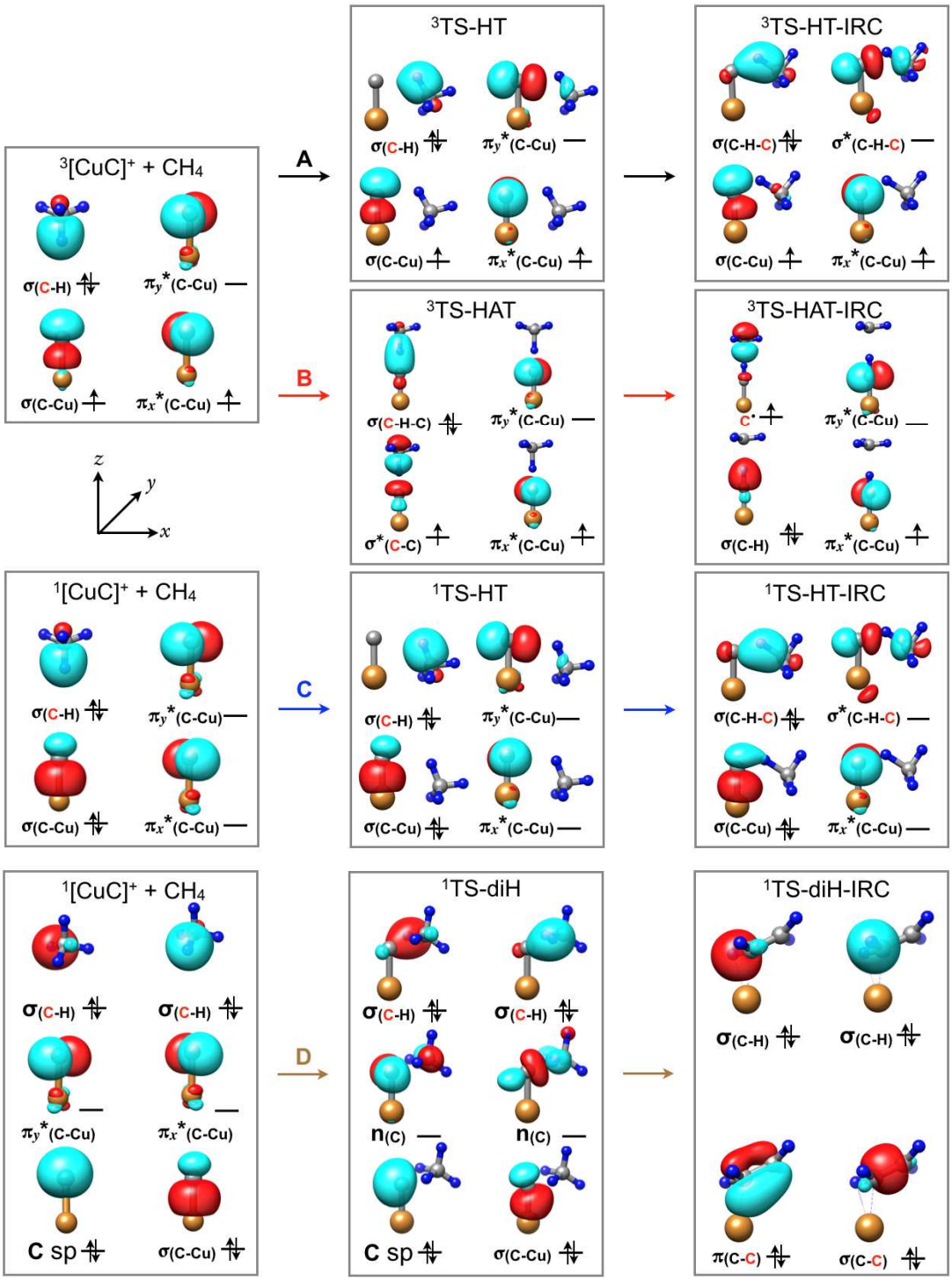

Figure S2. Schematic molecular orbital diagrams as represented by quasi-restricted orbitals for the C–H bond insertion steps in pathways **A**, **B**, **C**, and **D** (indicated in Figure S1a).

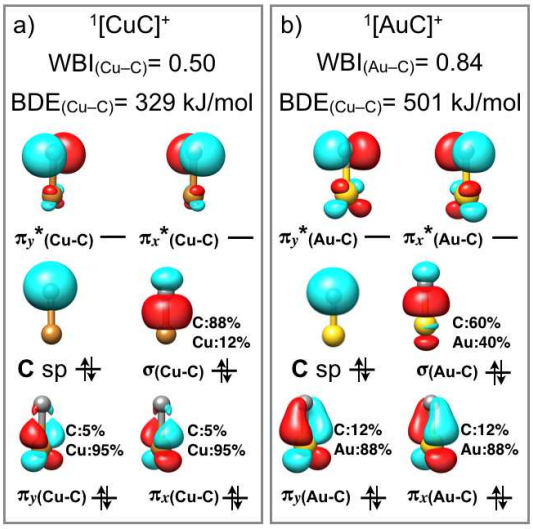

Figure S3. The orbital components, BDE, and Wiberg bond index (WBI) of (a) ^{1}[Cu–C]$^+$ and (b) ^{1}[Au–C]$^+$. Note that [Au–C]$^+$ is substantially more covalent than [Cu–C]$^+$.

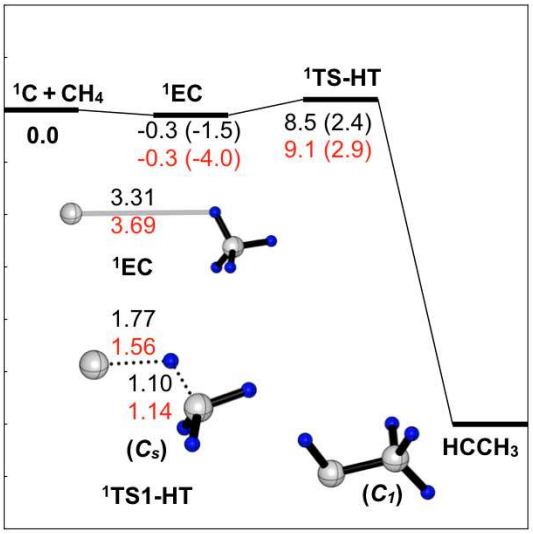

Figure S4. QCISD/cc-pVTZ and CCSD/cc-pVTZ-calculated potential energy profiles for the insertion of C(^{1}D) into a C-H bond of CH_4. Key ground-state structures with selected geometric parameters (in Å) are also provided. The zero-point vibration corrected energies (ΔH_{298K} in kJ mol^{-1}) or not (ΔE in kJ mol^{-1}) of the encounter complex and transition state are given relative to the separated reactants C(^{1}D) and CH_4. Color code: QCISD, black; CCSD, red. ΔH, in parentheses; ΔE, without parentheses.

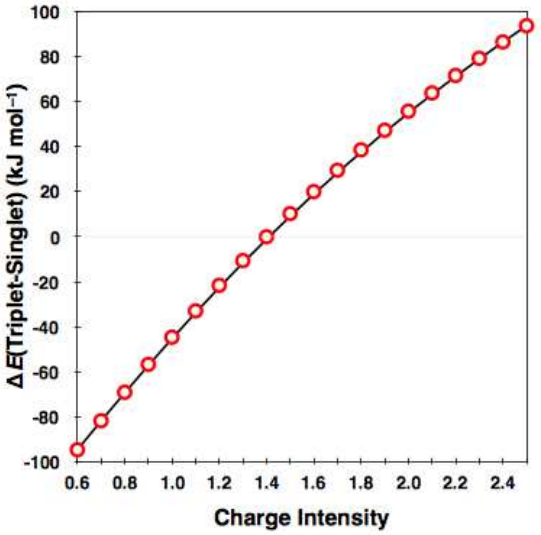

Figure S5. Energy gap (kJ mol^{-1}) between the triplet and singlet state of atomic carbon under the influence of a positive point charge at a distance of 1.76 Å, i.e. the distance of copper and carbon in the ground state $^{3}[Cu–C]^{+}$.

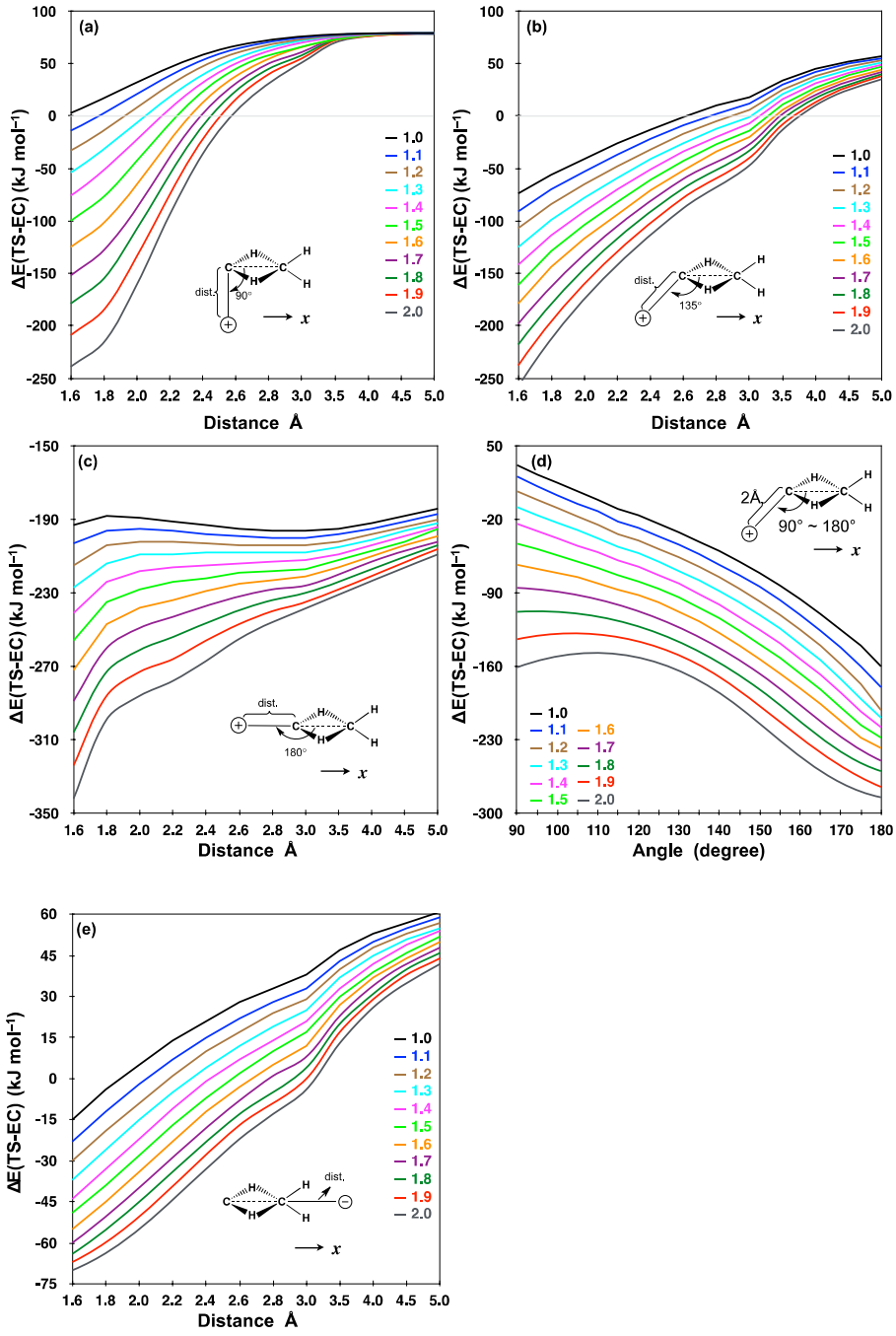

Figure S6. Plot of the relative energies (kJ mol^{-1}) between transition state and encounter complex under the influence of a positive point charge. Charge intensities (1.0e to 2.0e) are colored by black to gray. In a), b), c), distances between the positive point charge and C(^{1}D) are in the range of 1.6 Å to 5.0 Å; the angles ∢⊕–C–C = 90°, 135°, 180° respectively. In d), the distance between the point charge and C was set to 2.0 Å, the angle ∢⊕–C–C was scanned from 90° to 180°. In e) negative point charge is used; the same setup as in c).
Note that here the corresponding structures of the C(^{1}D) + CH_4 reaction are used.

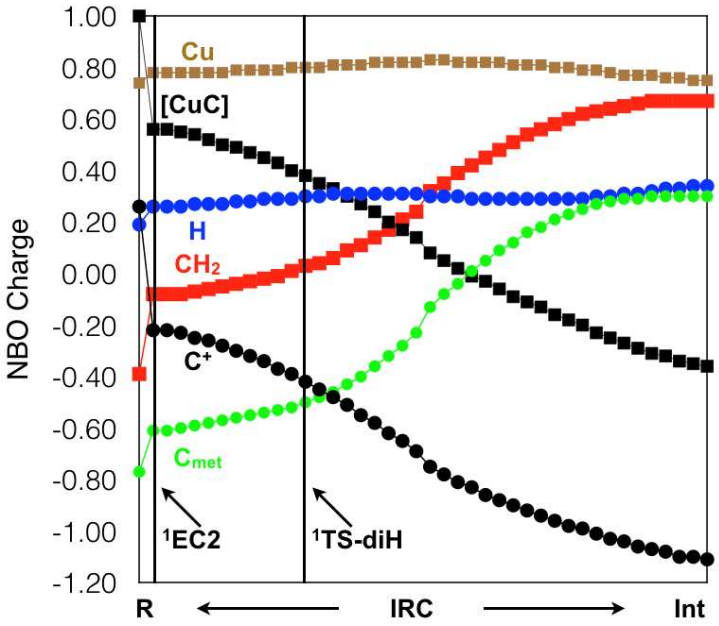

Figure S7. The evolution of the NBO charges along the reaction coordinate of the synchronous insertion of an electrophilic carbon atom into two C–H bonds of methane.

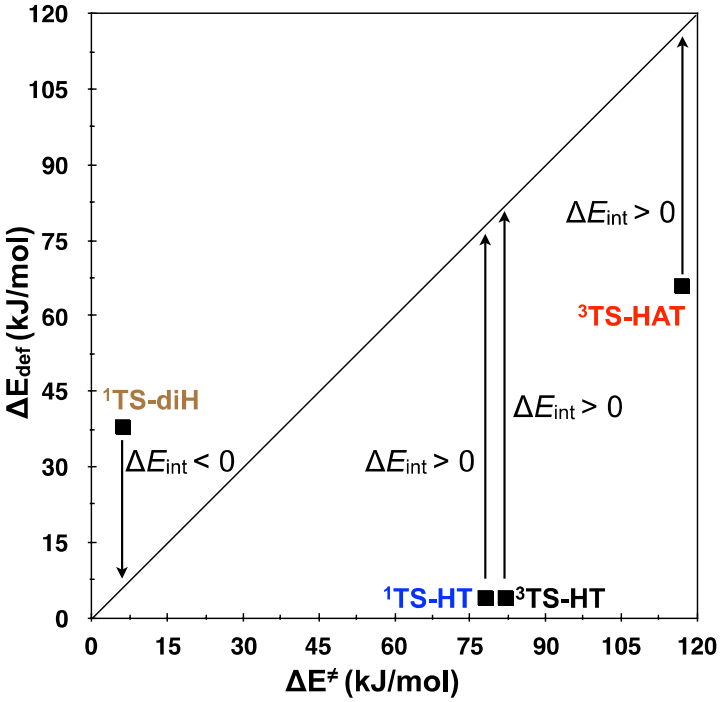

Figure S8. Plot of the sum of the deformation energies of the reactants in the TS (ΔE_{def}, kJ mol^{-1}) vs. the corresponding barriers $\Delta E^{\neq}$ (kJ mol^{-1}) relative to the encounter complexes. Note that only for the concerted reaction (via **^{1}TS-diH**) $\Delta E_{int} < 0$.

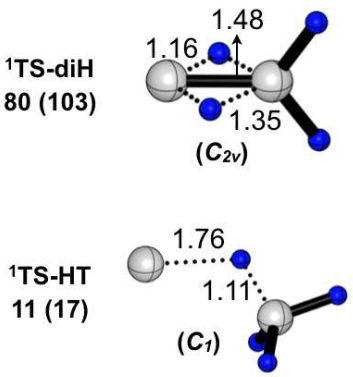

Figure S9. The B2PLYP/BSI optimized transition states for the insertion mechanisms into two and one C-H bond(s), respectively, for the reaction of C(^{1}D) + CH_4. Selected geometric parameters (in Å) are also provided. The zero-point vibration energy and thermal corrected energies (ΔH_{298K} in kJ mol^{-1}) or pure electronic structure energies (ΔE in kJ mol^{-1} in parentheses) of the transition states are given relative to the separated reactants C(^{1}D) and CH_4.

5. Tables

Table S1. Relative enthalpies and energies of the species involved in the reaction of $[Cu–C]^+$ + CH_4 related to the triplet ground state of the separated reactants (kJ mol^{-1}), at different levels.[a,b]

	$\Delta H_{ccsd\text{-}b2plyp}$	$\Delta H_{ccsd\text{-}b2gp}$	ΔH_{b2plyp}	ΔH_{b2gp}	$\Delta E_{ccsd\text{-}b2plyp}$	$\Delta E_{ccsd\text{-}b2gp}$	ΔE_{b2plyp}	ΔE_{b2gp}	ΔTh_{b2plyp}	ΔTh_{b2gp}	ΔZpe_{b2plyp}
$^3R + CH_4$	0	0	0	0	0	0	0	0	0	0	0
$^1R + CH_4$	14	14	17	28	14	14	16	14	1	1	1
$^1EC1$	-91	-89	-90	-88	-93	-92	-93	-92	2	3	4
$^3EC1$	-111	-110	-113	-118	-113	-113	-116	-113	2	3	4
^1EC	-56	-54	-56	-54	-52	-51	-52	-51	-4	-3	-1
$^1TS\text{-}HT$	-19	-18	-14	-11	-18	-18	-13	-18	-1	0	1
$^3TS\text{-}HT$	-40	-39	-37	-44	-37	-37	-34	-37	-3	-2	-1
$^3TS\text{-}HAT$	11	11	-8	-4	21	21	2	21	-10	-10	-6
$^1TS\text{-}diH$	-56	-55	-55	-57	-48	-48	-46	-48	-9	-7	-4
$^1I1$	-467	-461	-477	-478	-474	-466	-483	-466	7	5	12
$^3I1$	-319	-319	-327	-333	-324	-323	-332	-323	4	5	8
^1I	-632	-631	-627	-643	-645	-644	-640	-644	13	13	19
$^1TS1/2$	-467	-467	-468	-479	-469	-469	-470	-469	2	2	8
$^3TS1/2$	-121	-156	-174	-171	-121	-146	-175	-146	0	-10	6
$^3I2$	-290	-289	-286	-303	-303	-302	-299	-302	13	13	16
$^3TS2/3$	-219	-219	-236	-237	-207	-207	-224	-207	-12	-12	-7
$^3I3$	-227	-198	-244	-222	-221	-219	-238	-219	-6	21	-4
$^1TS1/3$	-211	-209	-215	-218	-200	-199	-204	-199	-10	-10	-6
$^3TS1/3$	-218	-217	-224	-232	-207	-207	-213	-207	-11	-10	-6
$^1I3$	-224	-176	-242	-200	-220	-219	-239	-219	-4	43	0
$^3TS3/4$	-97	-91	-120	-114	-74	-74	-97	-74	-23	-18	-20
$^3I4$	-116	-105	-135	-127	-93	-87	-111	-87	-23	-18	-22
$^3ts4/5$	-51	-49	-44	-31	-23	-23	-16	-23	-28	-26	-22
$^3I5$	-150	-155	-177	-177	-140	-139	-167	-139	-10	-15	-8
$^1P1$	-437	-436	-414	-429	-448	-446	-424	-446	10	11	26
$^3P1$	-180	-179	-174	-184	-191	-190	-185	-190	10	11	26
$^1P2$	-442	-442	-440	-448	-423	-423	-421	-423	-19	-19	-21
$^3P2$	-86	-86	-109	-104	-64	-64	-87	-64	-22	-23	-24
P3	-168	-168	-173	-184	-150	-150	-155	-150	-19	-18	-23

[a] Enthalpies are electronic structure energies with ZPVE and thermal corrections. Electronic structure energies are without ZPVE and thermal corrections

[b] $\Delta H_{ccsd\text{-}b2plyp}$ refers to enthalpies obtained with CCSD(T)/BSII//B2PLYP/BSI; $\Delta H_{ccsd\text{-}b2gp}$ refers to enthalpies obtained with CCSD(T)/BSII//B2GP-PLYP/BSI;

ΔH_{b2plyp} refers to enthalpies obtained with B2PLYP/BSI;

ΔH_{b2gp} refers to enthalpies obtained with B2GP-PLYP/BSI;

$\Delta E_{ccsd\text{-}b2plyp}$ refers to electronic structure energies obtained with CCSD(T)/BSII//B2PLYP/BSI;

$\Delta E_{ccsd\text{-}b2gp}$ refers to enthalpies obtained with CCSD(T)/BSII//B2GP-PLYP/BSI;

ΔE_{b2plyp} refers to enthalpies obtained with B2PLYP/BSI;

ΔE_{b2gp} refers to enthalpies obtained with B2GP-PLYP/BSI;

ΔTh_{b2plyp} refers to ZPVE and thermal corrections obtained with B2PLYP/BSI;

ΔTh_{b2gp} refers to ZPVE and thermal corrections obtained with B2GP-PLYP/BSI; ΔZpe_{b2plyp} refers to ZPVE obtained with B2PLYP/BSI.

Table S2. Experimental and calculated bond dissociation energies (in kJ mol^{-1}).

R	→	Educts	This work[a]	Previous work
$^3[Cu^+–C]$	→	$^1Cu^+ + C(^1D)$[b]	344.7	
$^1[Cu^+–C]$	→	$^1Cu^+ + C(^1D)$	328.8	
$^3[Cu^+–C]$	→	$^1Cu^+ + C(^3P)$		194.9[c]
$^1[Au^+–C]$	→	$^1Au^+ + C(^1D)$	500.9	
$^1[Au^+–C]$	→	$^1Au^+ + C(^1D)$		489.7[d]
$^1[Au^+–C]$	→	$^1Au^+ + C(^3P)$		≥ 307.8[e]
				324 ± 4[f]

[a], calculated at the B2PLYP/BSI level of theory;

[b] The lowest electronically excited state of atomic carbon, ^1D, is metastable with an energy content of 121.8 kJ mol^{-1} with respect to the ground ^3P state.[53]

[c], reference[49];

[d], reference[50];

[e], reference[51];

[f], reference[52].

Table S3. NBO-calculated charge and spin distributions of the transition states in the four reaction pathways of $[Cu–C]^+/CH_4$. C refers to the carbon atom of $[Cu–C]^+$; C_{met} refers to the carbon atom of methane; H_T refers to the hydrogen-atom in transit.

	$^1R + CH_4$	$^1TS\text{-}HT$	$^1TS\text{-}diH$	$^3R + CH_4$	$^3TS\text{-}HT$	$^3TS\text{-}HAT$
			Charge			
Cu	0.74	0.81	0.80	0.92	0.94	0.85
C	0.26	0.14	-0.42	0.08	-0.03	-0.05
C_{met}	-0.77	-0.84	-0.50	-0.77	-0.75	-0.53
H_T	0.19	0.20	0.30	0.19	0.18	0.09
H	0.19	0.21	0.30	0.19	0.15	0.21
H	0.19	0.28	0.25	0.19	0.24	0.21
H	0.19	0.20	0.27	0.19	0.27	0.21
			Spin			
Cu	0.00	0.00	0.00	0.14	0.11	0.08
C	0.00	0.00	0.00	1.86	1.88	1.40
C_{met}	0.00	0.00	0.00	0.00	0.01	0.63
H_T	0.00	0.00	0.00	0.00	0.00	-0.07
H	0.00	0.00	0.00	0.00	0.00	-0.01
H	0.00	0.00	0.00	0.00	0.00	-0.01
H	0.00	0.00	0.00	0.00	0.00	-0.01

Table S4. Trend of the relative energies (kJ mol^{-1}) as a function of charge intensity for the $\oplus$–C(^{1}D)/CH_4 reaction.

Charge	EC-SR[a]	TS-EC[b]	TS-SR[c]
0.10	-13.8	72.6	58.8
0.15	-15.1	69.4	54.3
0.20	-16.7	66.1	49.4
0.25	-18.5	62.6	44.1
0.30	-20.4	59.0	38.6
0.35	-22.6	55.2	32.6
0.40	-25.0	51.3	26.3
0.45	-27.5	47.2	19.6
0.50	-30.3	42.9	12.6
0.55	-33.3	38.4	5.1
0.60	-36.5	33.8	-2.7
0.65	-39.9	29.0	-10.9
0.70	-43.5	24.0	-19.6
0.75	-47.4	18.8	-28.6
0.80	-51.5	13.4	-38.1
0.85	-55.8	7.8	-47.9
0.90	-60.3	2.1	-58.2
0.95	-65.1	-3.9	-68.9
1.00	-70.1	-10.0	-80.1

[a], EC-SR, relative energies between encounter complex and separated reactants; [b], TS-EC, relative energies between transition state and encounter complex; [c], TS-SR, relative energies between transition state and separated reactants. The point charge is placed at the position of copper cation as that in ^{1}**TS-diH** of the $[Cu–C]^+/CH_4$ reaction. These values are calculated at the B2PLYP/cc-pVTZ level of theory.

Table S5. NBO-calculated charge distributions of the transition state **^{1}TS-diH** for the four reaction couples considered in this study, i.e. ^{1}[Cu–C]$^+$/CH_4, ^{1}[Au–C]$^+$/CH_4, C(^{1}D)/CH_4, and $\oplus$–C(^{1}D)/CH_4. M = Cu, Au; C = carbon atom that inserts into the two C–H bonds of methane; C_{met} = carbon atom of methane; H_t = hydrogen-atom(s) in transit; $\oplus$–C(^{1}D) = positive charge added to the carbon atom in its singlet ground state.

	^{1}[Cu–C]$^+$	^{1}[Au–C]$^+$	C(^{1}D)	$\oplus$–C(^{1}D)
M	0.80	0.58		
C	-0.42	-0.34	-0.79	-1.04
C_{met}	-0.50	-0.40	-0.20	-0.15
H_t	0.30	0.31	0.35	0.36
H_t	0.30	0.31	0.35	0.36
H	0.25	0.26	0.14	0.22
H	0.27	0.28	0.14	0.25

6. References

(1) Engeser, M.; Weiske, T.; Schröder, D.; Schwarz, H. *J. Phys. Chem. A* **2003**, *107*, 2855–2859.
(2) Schröder, D.; Schwarz, H.; Clemmer, D. E.; Chen, Y.; Armentrout, P. B.; Baranov, V. I.; Böhme, D. K. *Int. J. Mass. Spectrom.* **1997**, *161*, 175–191.
(3) Eller, K.; Schwarz, H. *Int. J. Mass. Spectrom.* **1989**, *93*, 243–257.
(4) Frisch, M. J.; Trucks, G. W.; Schlegel, H. B.; Scuseria, G. E.; Robb, M. A.; Cheeseman, J. R.; Scalmani, G.; Barone, V.; Mennucci, B.; Petersson, G. A.; Nakatsuji, H.; Caricato, M.; Li, X.; Hratchian, H. P.; Izmaylov, A. F.; Bloino, J.; Zheng, G.; Sonnenberg, J. L.; Hada, M.; Ehara, M.; Toyota, K.; Fukuda, R.; Hasegawa, J.; Ishida, M.; Nakajima, T.; Honda, Y.; Kitao, O.; Nakai, H.; Vreven, T.; J. A. Montgomery, J.; Peralta, J. E.; Ogliaro, F.; Bearpark, M.; Heyd, J. J.; Brothers, E.; Kudin, K. N.; Staroverov, V. N.; Keith, T.; Kobayashi, R.; Normand, J.; Raghavachari, K.; Rendell, A.; Burant, J. C.; Iyengar, S. S.; Tomasi, J.; Cossi, M.; Rega, N.; Millam, J. M.; Klene, M.; Knox, J. E.; Cross, J. B.; Bakken, V.; Adamo, C.; Jaramillo, J.; Gomperts, R.; Stratmann, R. E.; Yazyev, O.; Austin, A. J.; Cammi, R.; Pomelli, C.; Ochterski, J. W.; Martin, R. L.; Morokuma, K.; Zakrzewski, V. G.; Voth, G. A.; Salvador, P.; Dannenberg, J. J.; Dapprich, S.; Daniels, A. D.; Farkas, O.; Foresman, J. B.; Ortiz, J. V.; Cioslowski, J.; Fox, D. J. **Gaussian 09, Revision D.01, Gaussian, Inc., Wallingford CT, 2013.**
(5) Grimme, S. *J. Chem. Phys.* **2006**, *124*, 034108.
(6) Peterson, A. K.; Puzzarini, C. *Theor. Chem. Acc.* **2005**, *114*, 283-296.
(7) Dunning, T. H. *J. Chem. Phys.* **1989**, *90*, 1007–1023.
(8) Truhlar, D. G.; Gordon, M. S. *Science* **1990**, *249*, 491-498.
(9) Gonzalez, C.; Schlegel, H. B. *J. Phys. Chem.* **1990**, *94*, 5523-5527.
(10) Fukui, K. *Acc. Chem. Res.* **1981**, *14*, 363-368.
(11) Fukui, K. *J. Phys. Chem.* **1970**, *74*, 4161-4163.
(12) Jansen, G.; Hess, B. A. *Phys. Rev. A* **1989**, *39*, 6016-6017.
(13) Li, J.; Zhou, S.; Zhang, J.; Schlangen, M.; Weiske, T.; Usharani, D.; Shaik, S.; Schwarz, H. *J. Am. Chem. Soc.* **2016**, *138*, 7973–7981.
(14) Li, J.; Andrejić, M.; Mata, R. A.; Ryde, U. *Eur. J. Inorg. Chem.* **2015**, 3580–3589.
(15) Li, J. L.; Mata, R. A.; Ryde, U. *J. Chem. Theory Comput.* **2013**, *9*, 1799-1807.
(16) Kang, R. H.; Chen, H.; Shaik, S.; Yao, J. N. *J. Chem. Theory Comput.* **2011**, *7*, 4002-4011.
(17) Perdew, J. P.; Burke, K.; Ernzerhof, M. *Phys. Rev. Lett.* **1996**, *77*, 3865-3868.
(18) Zhao, Y.; Truhlar, D. *Theor. Chem. Acc.* **2008**, *120*, 215-241.
(19) Peverati, R.; Truhlar, D. G. *J. Phys. Chem. Lett.* **2011**, *2*, 2810-2817.
(20) Peverati, R.; Truhlar, D. G. *J. Phys. Chem. Lett.* **2012**, *3*, 117-124.
(21) Becke, A. D. *J. Chem. Phys.* **1993**, *98*, 1372-1377.
(22) Karton, A.; Tarnopolsky, A.; Lamère, J.-F.; Schatz, G. C.; Martin, J. M. L. *J. Phys. Chem. A* **2008**, *112*, 12868-12886.
(23) Head-Gordon, M.; Pople, J. A.; Frisch, M. J. *Chem. Phys. Lett.* **1988**, *153*, 503-506.
(24) Li, J.; Zhou, S.; Schlangen, M.; Weiske, T.; Schwarz, H. *Angew. Chem. Int. Ed.* **2016**, *55*, 13072–13075.
(25) Leonori, F.; Skouteris, D.; Petrucci, R.; Casavecchia, P.; Rosi, M.; Balucani, N. *J. Chem. Phys.* **2013**, *138*, 024311.
(26) Usharani, D.; Lacy, D. C.; Borovik, A. S.; Shaik, S. *J. Am. Chem. Soc.* **2013**, *135*, 17090-17104.
(27) Li, J.; Zhou, S.; Zhang, J.; Schlangen, M.; Usharani, D.; Shaik, S.; Schwarz, H. *J. Am. Chem. Soc.* **2016**, *138*, 11368–11377.
(28) Usharani, D.; Janardanan, D.; Li, C.; Shaik, S. S. *Acc. Chem. Res.* **2013**, *46*, 471–482.
(29) van Zeist, W.-J.; Bickelhaupt, F. M. *Org. Biomol. Chem.* **2010**, *8*, 3118-3127.
(30) Ess, D. H.; Houk, K. N. *J. Am. Chem. Soc.* **2008**, *130*, 10187–10198.
(31) Legault, C. Y.; Garcia, Y.; Merlic, C. A.; Houk, K. N. *J. Am. Chem. Soc.* **2007**, *129*, 12664-12665.
(32) Ess, D. H.; Houk, K. N. *J. Am. Chem. Soc.* **2007**, *129*, 10646-10647.

(33) Diefenbach, A.; Bickelhaupt, F. M. *J. Phys. Chem. A* **2004**, *108*, 8460-8466.
(34) Mitchell, D. J.; Schlegel, H. B.; Shaik, S. S.; Wolfe, S. *Can. J. Chem.* **1985**, *63*, 1642-1648.
(35) Ziegler, T.; Rauk, A. *Inorg. Chem.* **1979**, *18*, 1558-1565.
(36) Strozier, R. W.; Caramella, P.; Houk, K. N. *J. Am. Chem. Soc.* **1979**, *101*, 1340-1343.
(37) Kitaura, K.; Morokuma, K. *Int. J. Quantum. Chem.* **1976**, *10*, 325-340.
(38) Morokuma, K. *J. Chem. Phys.* **1971**, *55*, 1236-1244.
(39) Reed, A. E.; Curtiss, L. A.; Weinhold, F. A. *Chem. Rev.* **1988**, *88*, 899–926.
(40) Carpenter, J. E.; Weinhold, F. A. *J. Mol. Struc.-Theochem.* **1988**, *169*, 41–62.
(41) Reed, A. E.; Weinstock, R. B.; Weinhold, F. A. *J. Chem. Phys.* **1985**, *83*, 735–746.
(42) Reed, A. E.; Weinhold, F. A. *J. Chem. Phys.* **1985**, *83*, 1736–1740.
(43) Reed, A. E.; Weinhold, F. A. *J. Chem. Phys.* **1983**, *78*, 4066–4073.
(44) Foster, J. P.; Weinhold, F. A. *J. Am. Chem. Soc.* **1980**, *102*, 7211–7218.
(45) Glendening, E. D.; Badenhoop, J. K.; Reed, A. E.; Carpenter, J. E.; Bohmann, J. A.; Morales, C. M.; Landis, C. R.; Weinhold, F. **NBO 6.0**, Theoretical Chemistry Institute, University of Wisconsin, Madison, WI, 2013.
(46) Ye, S.; Geng, C.-Y.; Shaik, S.; Neese, F. *Phys. Chem. Chem. Phys.* **2013**, *15*, 8017-8030.
(47) Neese, F. *J. Am. Chem. Soc.* **2006**, *128*, 10213-10222.
(48) Neese, F. *WIREs Comput. Mol. Sci.* **2012**, *2*, 73-78.
(49) Ticknor, B. W.; Bandyopadhyay, B.; Duncan, M. A. *J. Phys. Chem. A* **2008**, *112*, 12355-12366.
(50) Barysz, M.; Pyykkö, P. *Chem. Phys. Lett.* **1998**, *285*, 398-403.
(51) Li, F.-X.; Armentrout, P. B. *J. Chem. Phys.* **2006**, *125*, 133114.
(52) Aguirre, F.; Husband, J.; Thompson, C. J.; Metz, R. B. *Chem. Phys. Lett.* **2000**, *318*, 466–470.
(53) Schofield, K. *J. Phys. Chem. Ref. Data* **1979**, *8*, 723.

7. Coordinates:

^{1}EC1
1 1 (Charge, Multiplicity)

Cu	0.264199	0.092349	−0.062755
C	2.028808	0.165658	−0.149519
C	−1.848425	−0.071947	−0.005559
H	−1.355323	−0.212878	0.980655
H	−1.913150	−1.001823	−0.567445
H	−2.846726	0.260283	0.271395
H	−1.475404	0.768674	−0.629906

^{3}EC1
1 3

Cu	0.453928	0.565046	0.161071
C	−1.275497	0.919577	0.383161
C	2.538831	0.137670	−0.106617
H	1.769135	−0.542594	−0.546400
H	2.224368	1.040361	0.472056
H	3.121249	−0.469954	0.577468
H	3.126626	0.505286	−0.940735

^{1}EC
1 1

Cu	−0.338816	−0.002877	−0.664083
C	−0.305178	0.002981	1.156133
C	1.417764	0.001793	1.833760
H	0.952001	−0.937911	1.389011
H	2.422000	−0.004129	1.396115
H	0.959028	0.944075	1.389737
H	1.368196	0.001901	2.913767

MECP
1 1/3

Cu	−0.084044	0.000000	−0.114399
C	−0.056574	0.000000	1.703101
C	1.749496	0.000000	2.535383
H	1.254913	−0.948852	2.204053
H	2.732374	0.000000	2.064624
H	1.254913	0.948852	2.204053
H	1.731957	0.000000	3.619978

^{1}TS-diH
1 1

Cu	0.019799	0.000000	−0.008930
C	0.023477	0.000000	1.820126
C	1.672397	0.000000	2.432308
H	0.965954	−0.926581	2.372491
H	2.539109	0.000000	1.783899
H	0.965954	0.926581	2.372491
H	1.867858	0.000000	3.508061

^{3}TS-HT
1 3

Cu	0.635508	−0.167638	0.504267
C	−0.010781	1.393430	−0.143105
C	−2.059120	−0.244264	−0.090237
H	−1.999217	−0.634360	−1.099586
H	−1.831657	0.840178	−0.083747
H	−3.069324	−0.320029	0.311088
H	−1.425399	−0.827125	0.600840

^{1}TS-HT
1 1

Cu	0.587028	0.048741	−0.575043
C	0.459763	1.265732	0.687590

C	-2.014846	-0.086353	-0.028187
H	-1.700506	0.767478	0.589139
H	-1.614085	-1.030112	0.343272
H	-3.099998	-0.125171	0.076839
H	-1.816420	0.065492	-1.093562

^{3}TS-HAT
1 3

Cu	-0.674326	0.000232	-0.000288
C	1.097048	0.001895	-0.001187
C	3.774981	-0.000264	0.000148
H	2.451182	0.004418	-0.002875
H	3.998369	-0.300674	1.016872
H	4.003740	-0.735092	-0.762009
H	4.012245	1.026545	-0.248072

^{1}I
1 1

Cu	0.138125	0.115706	0.735913
C	-0.388055	-1.287719	-0.686534
C	0.498814	-1.847275	0.200582
H	-1.456657	-1.417718	-0.563028
H	1.559251	-1.882599	-0.019153
H	0.149801	-2.431338	1.043864
H	-0.047134	-0.869033	-1.625971

^{1}I1
1 1

Cu	0.923112	0.227593	-0.303177
C	-0.616667	0.546898	0.635859
C	-1.954915	0.116104	0.350944
H	-0.531938	1.078904	1.585197
H	-1.935136	-0.782138	1.027297
H	-2.744985	0.736256	0.775954
H	-2.161416	-0.245597	-0.649054

^{3}I1
1 3

Cu	0.692994	0.060011	-0.327219
C	-0.967727	0.845325	-0.060171
C	-2.192419	0.060713	-0.202991
H	-2.098929	-0.785898	-0.887182
H	-0.797621	1.837415	0.352890
H	-2.967287	0.715721	-0.623322
H	-2.542067	-0.320351	0.761517